Surface Plasmon Coupling of Compositionally Heterogeneous Core–Satellite Nanoassemblies

ARTICLE *in* JOURNAL OF PHYSICAL CHEMISTRY LETTERS · APRIL 2013

Impact Factor: 7.46 · DOI: 10.1021/jz400602f

5 AUTHORS, INCLUDING:

Martin G Blaber

Seagate Technology

36 PUBLICATIONS **911** CITATIONS

SEE PROFILE

THE JOURNAL OF PHYSICAL CHEMISTRY Letters

Letter

pubs.acs.org/JPCL

Surface Plasmon Coupling of Compositionally Heterogeneous Core–Satellite Nanoassemblies

Jun Hee Yoon,[†,§] Yong Zhou,[‡,§] Martin G. Blaber,[‡] George C. Schatz,*[,‡] and Sangwoon Yoon*[,†]

[†]Department of Chemistry, Institute of Nanosensor and Biotechnology, Dankook University, 152 Jukjeon-ro, Suji-gu, Yongin, Gyeonggi 448-701, Korea

[‡]Department of Chemistry, Northwestern University, 2145 Sheridan Road, Evanston, Illinois 60208-3113, United States

Supporting Information

ABSTRACT: Understanding plasmon coupling between compositionally heterogeneous nanoparticles in close proximity is intriguing and fundamentally important because of the energy mismatch between the localized surface plasmons of the associated nanoparticles and interactions beyond classical electrodynamics. In this Letter, we explore surface plasmon coupling between silver nanoparticles (AgNPs) and gold nanoparticles (AuNPs), assembled in the form of core–satellite structures. A recently developed assembly method allows us to prepare ultrapure core–satellite nanoassemblies in solution, where 50 nm AgNPs are surrounded by 13 nm AuNPs via alkanedithiol linkers. We observe changes in the plasmon coupling between the AgNP core and AuNP satellites as the core-to-satellite gap distance varies from 2.3 to 0.7 nm. Comparison with theoretical studies reveals that the traditional hybridized plasmon modes are abruptly replaced by charge-transfer plasmons at a ∼1 nm gap. Changes with the number of satellites are also discussed.

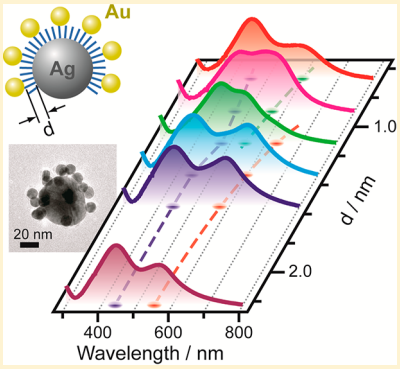

SECTION: Plasmonics, Optical Materials, and Hard Matter

Noble metal nanoparticles have unique optical properties arising from localized surface plasmon resonance (LSPR).[1] The collective oscillation of the conduction electrons in the nanoparticles upon irradiation leads to exceedingly large absorption or scattering of light by the nanoparticles, the generation of highly focused electric fields around the nanoparticles, and the emission of localized heat. These plasmonic properties have been utilized in increasing the resolution of sensing and imaging techniques as well as in photothermal therapeutics, solar energy conversion, and various surface-enhanced spectroscopies.[2−6] For many applications, the tunability of the LSPR is of paramount importance, which is often dictated by the size, shape, and materials involved, as well as the dielectric medium surrounding the nanoparticles.[1] Another appealing way to tune the LSPR frequency is to assemble nanoparticles into aggregates or assemblies.[7] When the constituent particles are brought into close proximity, interparticle interactions shift the LSPR frequency. The direction and extent of the frequency shift is highly tunable depending on how a given set of nanoparticles is assembled. The resonance frequency can be finely tuned by controlling the interparticle distances, relative orientation of coupled nanoparticles, and the number of nanoparticles constituting the assembly.[8−15]

Assembling nanoparticles in a controlled fashion is still a great challenge.[9,16,17] The assembled structures must be well-defined, reproducible, stable, and dispersible in solution for versatility. It should be easy to change the interparticle distances over a wide range, and the component nanoparticles should be readily replaceable by particles with different shapes, sizes, and materials.

Many of the previous assembly methods have produced a mixture of assemblies along with unassembled monomer particles, requiring postassembly separation processes.[18−21] The resulting nanoassemblies often have poorly defined structures. This inhomogeneity makes it difficult to interpret ensemble measurements in terms of the optical response of single assemblies.

Recently, we have developed a new assembly method that produces core–satellite assemblies of gold nanoparticles (AuNPs) with 100% purity, requiring no purification processes.[22] The prepared nanoassemblies have well-defined core-to-satellite gap distance (d), controlled by a self-assembled monolayer (SAM) of alkanedithiol linkers. By varying the length of the linkers, we modified the plasmon coupling between the core and satellite AuNPs as a function of the gap distance in the region of $d < 3$ nm. The stepwise assembly process in our method also provides great flexibility in changing the constituent nanoparticles and the number of satellites. These strengths of the new assembly scheme allow us to prepare compositionally heterogeneous core–satellite nanoassemblies in a controlled fashion which are otherwise difficult to attain. We explore the plasmon coupling that occurs in the nanoassemblies both experimentally and theoretically.

Received: March 19, 2013
Accepted: April 8, 2013
Published: April 8, 2013

   dx.doi.org/10.1021/jz400602f | J. Phys. Chem. Lett. 2013, 4, 1371−1378

Heterogeneous assembly structures are fascinating because they allow us to examine how the energy mismatch of the interacting nanoparticles influences the plasmon coupling. For instance, isolated AuNPs and isolated silver nanoparticles (AgNPs) have a dipole LSPR mode at ~520 nm (~2.4 eV) and ~410 nm (~3.0 eV), respectively. It is intriguing from a fundamental point of view how these energetically separated modes interact as the interparticle gap narrows and as the number of constituting nanoparticles increases. In addition, from a practical point of view, the coupling of these two different nanoparticles will provide a broader range of resonance frequencies, which is useful for more effective excitation of near-field effects that are important in surface-enhanced Raman scattering,[23] surface-enhanced fluorescence,[24] and plasmonic photocatalytic activity.[25]

Studies of heterogeneous assemblies, particularly with a focus on the structure-dependent plasmonic properties, are rare. Most systems previously studied are limited to heterodimers. Alivisatos and coworkers produced Ag–Au dimers using DNA linkers and observed plasmon coupling for a single assembly.[26] Notably, they found that the parallel antibonding mode has lower excitation energy than the LSPR mode of isolated AgNPs, contrary to what the plasmon hybridization model predicts.[13,14,27] The red-shift was attributed to the coupling of the AgNP LSPR mode with interband absorption processes in the AuNPs. Theoretical studies, pioneered by Brevet and coworkers, also revealed that such interactions between the discrete LSPR mode of AgNPs and the continuum interband transition (IBT) spectrum of AuNPs give rise to a Fano resonance profile in the absorption spectrum of gold.[28–31]

Our assembly method enables us to explore the coupling of surface plasmons in more complex heterogeneous nanoassemblies beyond dimers. We prepare Ag core–Au satellite nanoassembly structures with interparticle distances defined by alkanedithiol SAMs. Utilizing a stepwise assembly process, we can control the interparticle distances and the number of AuNP satellites. The measured optical responses of the Ag core–Au satellite nanoassemblies are compared with theoretical calculations using the generalized multiparticle Mie (GMM) theory, and we find that the results provide unique insights into the nature of the plasmon coupling of this nanostructure. In particular, we show the appearance of new plasmonic modes when the particle separation distance is small enough that electrons are able to transfer between the particles, either by tunneling or through a bridge. While this regime of particle coupling has been the subject of past theoretical studies (and some experiments),[32–34] the present results provide a particularly clear example of this effect.

Plasmon Coupling of Ag Core–Au Satellite Nanoassemblies. Plasmonic properties were first investigated for the core–satellite nanoassemblies with 1,10-decanedithiol linkers. The Ag core–Au satellite nanoassemblies were prepared using the selective desorption approach. (See the Experimental and Theoretical Methods.) The prepared Ag core–Au satellite nanoassemblies have similar structural features to their Au–Au counterparts reported previously.[22] A large AgNP (50 nm) is surrounded by 14 ± 3 satellite AuNPs (13 nm). A representative transmission electron microscopy (TEM) image is presented in the inset of Figure 1a.

We measured the extinction spectra of the Ag core–Au satellite nanoassemblies and compared them with those of the individual AgNPs and AuNPs (Figure 1a). The isolated AgNPs and AuNPs exhibit characteristic LSPR bands at 424 and 520 nm, respectively. When these nanoparticles are assembled into the core–satellite structures by the SAMs of 1,10-decanedithiol linkers, two peaks appear in the extinction spectrum: one at 444 nm and the other one at 591 nm, designated as "blue" band and "red" band, respectively, for convenience. Both of them are red-shifted from respective component LSPR bands.

This red-shift of the extinction band of an assembly, relative to the LSPR bands of their component nanoparticles, is commonly found in compositionally homogeneous nanoassemblies such as AuNP dimers and AuNP core–satellite nanostructures.[10–12,22] The LSPR modes of individual nano-

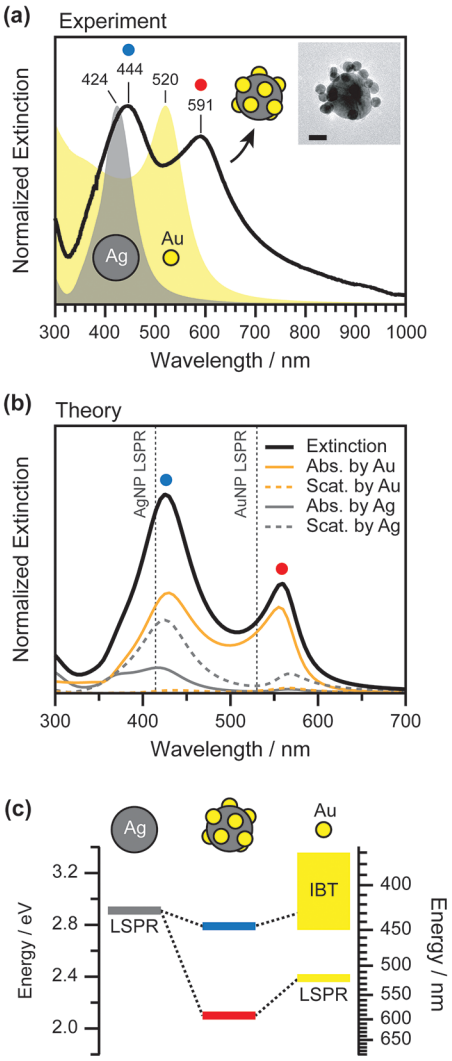

Figure 1. Plasmon coupling of Ag core–Au satellite nanoassemblies. (a) Extinction spectrum of the Ag core–Au satellite nanoassemblies prepared by using 1,10-decanedithiol linkers. Blue and red circles mark the "blue" and "red" bands, respectively. The structure of the assembly is represented by a TEM image in the inset (scale bar = 20 nm). The LSPR spectra of AgNPs and AuNPs used for the assembly are included in the spectrum for comparison. (b) Theoretical extinction spectrum calculated for the nanoassembly with the same structure as in panel a. For analysis, the extinction spectrum was decomposed into the absorption (solid line) and scattering (dashed line) by the AuNPs (yellow color) and AgNPs (gray color) in the assembly. For comparison, the calculated LSPR frequencies of AgNPs (50 nm) and AuNPs (13 nm) are marked by dotted lines. (c) Coupling diagram for the two extinction bands ("blue" and "red") of the Ag core–Au satellite nanoassemblies.

dx.doi.org/10.1021/jz400602f | J. Phys. Chem. Lett. 2013, 4, 1371–1378

particles, closely located in energy, are likely to mix and to form hybridized modes upon assembly.[13,14,27] Dipole-allowed transitions to lower energy, stabilized hybridization modes result in the red-shift of the extinction band of the assemblies from the LSPR bands of the component nanoparticles.

In contrast, the energy mismatch of the component LSPR modes in compositionally heterogeneous nanoassemblies complicates the interpretation of the coupling bands. Figure 1c presents a modified plasmon hybridization picture for Ag core−Au satellite nanoassemblies, adopted from the model proposed by Alivisatos and coworkers in their study of Ag−Au heterodimers.[26] Following this picture, we propose that the off-resonant coupling between the AgNP LSPR and AuNP LSPR gives rise to the "red" band at 591 nm. On the other hand, it is the resonant interaction of the LSPR of the AgNP with the IBT of AuNPs that produces the "blue" band at 444 nm.

Theoretical studies provide further insights into the nature of the couplings. Figure 1b shows that simulation using the GMM theory reproduces the experimental extinction spectrum reasonably well. We decomposed the simulated extinction spectrum into the absorption and scattering of each component AgNP and AuNPs in the assembly. The results show that the "red" band is mostly attributed to the absorption by the LSPR of AuNPs, which is red-shifted from the LSPR of isolated AuNPs. Notably, there is an additional contribution from the scattering of AgNP. Despite the off-resonance condition, the AgNP contributes to the "red" band through the scattering induced by the radiating electromagnetic field from the surrounding satellite AuNPs, which strongly absorb at this wavelength.[29] In other words, the LSPR excitation of AgNPs in the "red" band region is mediated by the LSPR of AuNPs. This result confirms the coupling of the LSPR of AuNPs with that of AgNPs in this spectral region.

The "blue" band consists of the dipolar LSPR excitation (absorption and scattering) of the AgNP and the continuum IBT absorption by the AuNPs. The red-shift caused by the interaction between the discrete LSPR mode of the AgNP and the continuum IBT mode of the AuNPs is consistent with the observation made by Alivisatos and coworkers for Ag−Au dimers.[26]

We also note that the Fano resonance profile at the far blue end of wavelength range considered here is not evident in the absorption spectrum of AuNPs in contrast with the previous studies (e.g., Figure 1 in ref 28). This results from the orientational averaging of contributions from all Ag core−Au satellite pairs. (A detailed discussion of this effect can be found in the Supporting Information.)

Changes in Plasmon Coupling with Variation in Core−Satellite Gap Distances. The plasmon coupling between the AgNP core and AuNP satellites must change with the gap distance between the core and the satellites, as is found for other coupled nanoparticle systems.[10−12,32,35,36] To explore the effect of gap distance on the plasmon coupling, we produced Ag core−Au satellite nanoassemblies with different interparticle gap distances using various lengths of alkanedithiol, $SH(CH_2)_nSH$ (n = 2, 4, 6, 8, 10, 16; abbreviated as *Cn* hereafter) in Step 3 of the assembly process. (See Experimental and Theoretical Methods.) Representative TEM images of each assembly are presented in the Supporting Information.

Figure 2a shows the optical responses of the Ag core−Au satellite nanoassemblies with varying linkers from *C16* to *C2*. Each spectrum was deconvoluted with Gaussian functions to reveal spectral features underlying the broad extinction spectra.

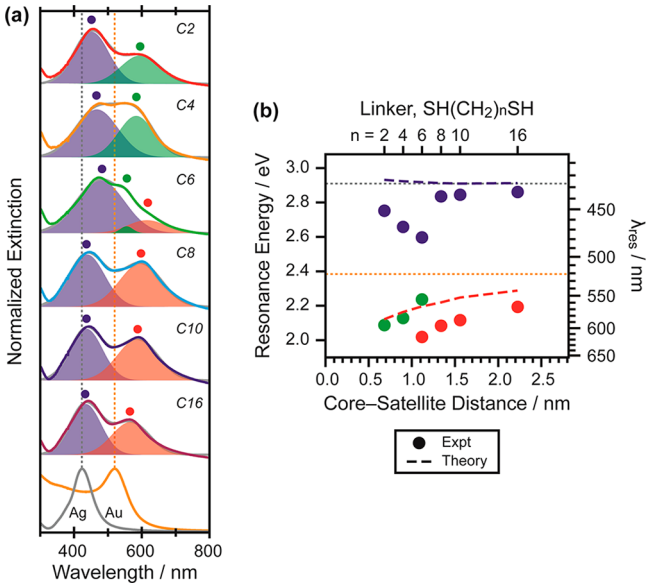

Figure 2. Changes in plasmon couplings with the core-to-satellite interparticle distances. (a) Extinction spectra of the Ag core−Au satellite nanoassemblies with the selected alkanedithiol linkers, $SH(CH_2)_nSH$ (*Cn*). The Gaussian functions used for deconvolution of the spectra are indicated by blue, green, and red colors. (b) Spectral positions of extinction bands in units of electronvolts and nanometers as a function of the core-to-satellite gap distances. The LSPR frequencies of isolated AgNPs (50 nm) and AuNPs (13 nm) are marked by gray and yellow horizontal dotted lines, respectively. The dashed lines indicate the peak positions of calculated extinction spectra of the nanoassemblies based on GMM theory.

The peak wavelengths of each Gaussian component are marked with circles in Figure 2a and plotted as a function of the core-to-satellite gap distance (d) in Figure 2b. The gap distances, defined by the height of the SAMs of the alkanedithiol linkers, were calculated using density functional theory, as previously discussed.[22] Note that it is difficult and often misleading to derive interparticle distance using TEM images for complex nanoassembly structures (Supporting Information).

Figure 2 shows that the "red" band progressively red-shifts as the core−satellite interparticle distance decreases from 2.2 (*C16* linker) to 1.3 nm (*C8* linker). The distance-dependent red-shift of the plasmon coupling band has been widely observed for dimers[10−12,32,37] and adopted as a plasmon ruler to measure the interparticle distances with Angstrom accuracy.[35,36,38] Analogous to the molecular orbital theory, the energy of the in-phase bonding mode of the hybridized dipolar surface plasmon modes is lowered as the coupling becomes stronger.

The "blue" band, on the other hand, shows only a slight, almost negligible, red-shift with decreasing distance going down to the *C8* linker (Figure 2b). This suggests that the coupling between the AgNP LSPR mode and the localized bound electrons in the AuNP is weak and only slightly amplified as distance is decreased.

A comparison of the experimental results with GMM theory in this coupling regime (d > 1.3 nm) shows that the theory underestimates the extent of the red-shifts for the "red" band, and produces a flat response for the "blue" band as opposed to a slight red-shift in the measured spectrum (Figure 2b). These deviations between experimental and GMM results may be attributed to two effects associated with the alkanedithiol

dx.doi.org/10.1021/jz400602f | J. Phys. Chem. Lett. 2013, 4, 1371−1378

linkers used in experiment that are not included in current GMM calculations. First, there are changes in the surrounding dielectric function of the Ag core (refractive index changing from 1.36 for ethanol to 1.42). Second, chemical interaction between Ag and the dithiolate linker molecules modifies the effective dielectric constant at the metal−thiolate interface, as shown in a previous study where it led to red-shifted plasmons compared with a theory that ignored the effect.[39] Both of these factors will red-shift the "red" and "blue" bands compared with what is described by GMM theory (as we have applied it). Furthermore, these two effects become more important as linker length is decreased because the near-field becomes more localized into the gap between the particles where the dielectric constant differs the most from what we have assumed in GMM. This therefore provides a mechanism whereby the "blue" band switches from a flat function to weak red-shifting, better reproducing the experimental "blue" band.

As the core-to-satellite gap distance is reduced to ∼1 nm, drastic changes occur to the extinction spectra of the Ag core−Au satellite nanoassemblies. When *C6* is used as a linker (d = 1.1 nm), a new band appears between the "blue" and "red" band, which we designate as the "green" band. Furthermore, the "blue" band suddenly red-shifts and broadens going from *C8* to *C6*, while the "red" band continues to red-shift but with its relative intensity significantly diminishing. As the interparticle distance becomes even shorter, the "green" band begins to red-shift while the "blue" band shifts in the opposite direction to the "green" band (Figure 2b).

The strong coupling between the core AgNPs and satellite AuNPs for interparticle distances less than ∼1 nm does not seem to fit to the classical electrodynamics model. Indeed, our GMM simulations show a continuing red-shift of the "red" band and a slight blue-shift of the "blue" band (dashed lines in Figure 2b). Recently, several methods have been developed to include effects that go beyond what is described by classical electrodynamics simulations for interacting spheres. One approach keeps with the classical electrodynamics description but adds a conducting bridge between the spheres.[32] In this case, it is found that even a very thin bridge leads to a profound change in the extinction spectra of coupled silver nanoparticles, with the red-shifting "bonding" mode now blue-shifting as the particles approach and a new mode appearing in the infrared that blue-shifts into the visible as the particle separation decreases. Another approach introduces quantum effects into the description of two interacting spheres or cylinders (but no bridge) by adding nonlocality into the dielectric function of the metal.[33,40−42] In these calculations, one finds that the "bonding" mode shifts red by smaller amounts compared with what is obtained from the local theory. This means that the bonding mode is to the blue of the local theory prediction, but it still red-shifts and diminishes in intensity as the two particles come together. A third option is to do a full quantum treatment of a dimer of particles using jellium and TDDFT.[34,43,44] In this case, however, one is forced to use small metal clusters rather than nanoparticles. Esteban et al.[34] have recently developed a continuum model involving a bridge between the spheres that mimics their quantum results for clusters and allows studying larger nanoparticles. They found that when the wave functions on the two particles overlap sufficiently, tunneling between the particles occurs, and this leads to two effects. One is that the bonding mode shifts red by smaller amounts than is obtained from local dielectric theory and with diminished intensity, basically giving the same result as from the nonlocal dielectric model of McMahon et al.[33] The other is that new modes appear, denoted as charge-transfer plasmons (CTPs) by Esteban et al.[34] The CTP modes are associated with the bridge between the two particles, much like the previous bridge model results.[32] The lowest energy CTP mode shows up in the infrared and blue-shifts as the particles approach. A second CTP, denoted CTP′, is slightly blue of the "bonding" mode, and it shifts blue as the particles approach. Higher order CTPs appear at higher energies and have similar dependence on separation.

On the basis of these theoretical studies, it is possible to assign the modes in Figure 2. We first note that there is no evidence of the low-energy CTP mode mentioned above, perhaps because it is too low in energy to be observed in our measurements. Instead, the lowest observed energy band is clearly the continuation of the bonding mode for larger distances but with a red-shift that is suppressed compared to local theory and with an intensity that diminishes such that it is not visible below *C6*. This behavior is precisely what is obtained from either the McMahon or the Esteban analysis. The "green" band in Figure 2 is apparently the CTP′ mode mentioned above, with the one disagreement between theory and experiment being that theory says it should slightly blue-shift as the particles approach, whereas the experiment says that it slightly red-shifts. On the basis of the discussion above, one could imagine that whether the shift is red or blue for this mode is a subtle function of how the bridge changes with separation (a shorter bridge would lead to blue-shifts, but this could be balanced by a higher electron density on the bridge that would lead to red-shifts), so this deviation between theory and experiment could easily occur. Finally, the "blue" band transition switches to a higher energy CTP at the *C6* separation; then, this band blue-shifts with decreasing separation, matching the behavior found by Esteban et al. for higher modes in the larger particles they studied.

For more accurate assignments, single-particle spectroscopy in combination with quantum simulations is required.[45,46] Also, studies of silver−gold dimers rather than core−satellite structures would reduce the structural complexity and presumably solidify the somewhat tentative assignments that we have provided in this Letter.

Changes of Plasmon Coupling with the Number of Satellites. Another factor affecting the plasmon coupling in the core−satellite assembly structure is the number of satellites (N_{sat}). For example, theoretical and experimental studies revealed that the plasmon coupling of Au core−Au satellite nanoassemblies almost linearly red-shifts with increasing satellite numbers.[47,48] In our experiments, the number of satellites is controlled by the time allowed for the thiol-functionalized core AgNPs on the glass slides to interact with the AuNPs in solution in step 4 of the assembly process. Figure 3a shows representative TEM images of the assemblies formed by immersing the core-adsorbed glass slides in the satellite AuNP solutions for the indicated time periods. We used *C10* as a linker. The number of satellites increases with immersion time, reaching an asymptotic value after an 1 h or so (Figure 3b). Adsorption of the satellite AuNPs on the core AgNPs follows pseudo-first-order kinetics with a limited number of binding sites on the core AgNPs and an excessive number of satellite AuNPs available in solution.[49] An exponential fit of the increase in the number of satellites with time yields the apparent rate constant of $(5.3 \pm 0.9) \times 10^{-2}$ min^{-1} and an asymptotic value of 14 ± 1. The adsorption kinetics are comparable with that of Au core−Au satellite

dx.doi.org/10.1021/jz400602f | J. Phys. Chem. Lett. 2013, 4, 1371−1378

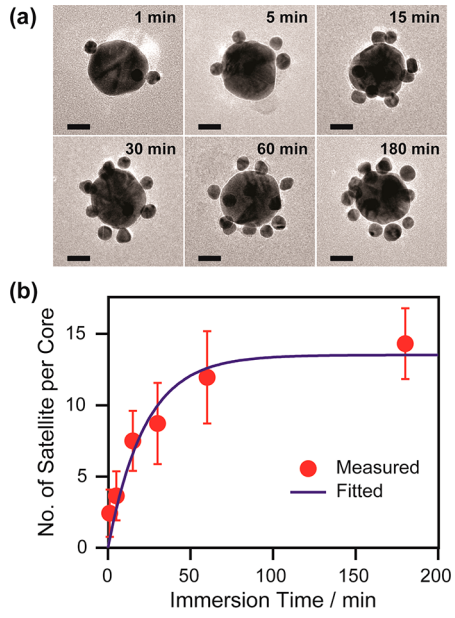

Figure 3. Control of the number of satellites. (a) Representative TEM images of the Ag core−Au satellite nanoassemblies formed by using the indicated immersion time in step 4 of the assembly process. The scale bars indicate 20 nm. (b) Plot of the number of satellites as a function of the immersion time. The error bars are one standard deviation from at least 76 assemblies. The solid line is the best fitted exponential function.

assemblies, where $(5.0 \pm 1.2) \times 10^{-2}$ min^{-1} and 14 ± 1 were reported for the rate constant and the asymptotic value, respectively.[48]

Extinction spectra of the Ag core−Au satellite nanoassemblies for different numbers of satellites show that the relative intensity of the "red" band to the "blue" band increases as the number of AuNP satellites increases (Figure 4a). Furthermore, both "blue" and "red" bands gradually red-shift with increasing numbers of satellites, although the changes in the latter are much larger than the former. More quantitative analysis reveals that the spectral shifts correspond to 1.6 ± 0.1 nm/satellite for the "red" band and 0.9 ± 0.2 nm/satellite for the "blue" band (Supporting Information).

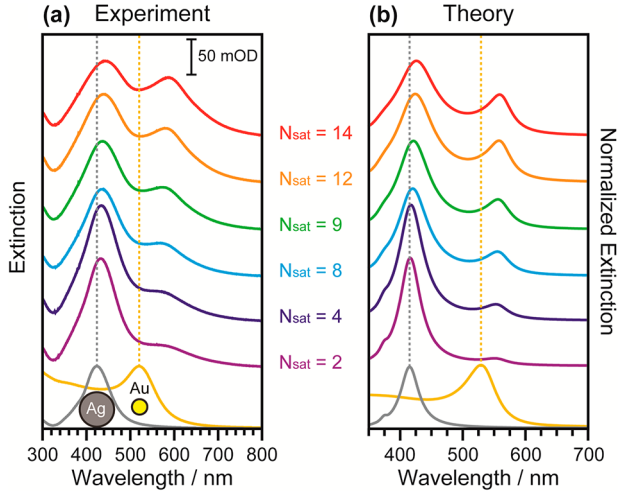

Figure 4. Evolution of the (a) measured and (b) calculated extinction spectra of the Ag core−Au satellite nanoassemblies with increasing number of satellites (N_{sat}).

Calculations using the GMM theory yield extinction spectra that qualitatively agree with the experimental ones (Figure 4b). For a more detailed analysis, total extinction spectra of the core−satellite nanoassemblies were decomposed into contributions of the core AgNP and the satellite AuNPs that constitute the assemblies. Figure 5a shows that the decrease in the intensity of the "blue" band with the increasing number of AuNP satellites is mostly due to the optical response of the core AgNP. The loss of the absorption and scattering of AgNP as it is coupled to more satellite AuNPs is greater than the gain of the IBT absorption of the AuNPs and therefore the overall intensity decreases in this spectral region. In contrast, in the "red" band region, both the LSPR absorption of AuNPs and the induced scattering of AgNPs increase as more satellite AuNPs surround the core AgNP (Figure 5b).

Furthermore, our calculations reveal the origins of the red-shifts of the "blue" and "red" bands. Figure 5c,d shows that the optical responses of both AgNP and AuNPs red-shift with increasing number of AuNP satellites, contributing to the red-shift of the overall extinction spectra. The more significant red-shift in the "red" band region is primarily due to the large red-shift of the scattering of AgNP, induced by more AuNPs around it.

In conclusion, we explored the surface plasmon coupling of core−satellite nanostructures where the AgNP (50 nm) at the core is connected to a definite number of AuNPs (13 nm) by alkanedithiol linkers. The nanoassemblies were prepared in a dispersed solution state with ultrahigh purity using a controlled assembly method based on the selective desorption. Even though the LSPR modes of AgNPs (λ = 424 nm) and AuNPs (λ = 520 nm) are distant in energy, the bonding dipolar coupling band was observed as red-shifted from the LSPR band of AuNPs. This "red" band continually red-shifts as the interparticle distance between the core and the satellites decreases to ∼1 nm. Resonant interaction of the LSPR mode of AgNPs with the continuum IBT mode of AuNPs also produces a coupling band, here being red-shifted from the LSPR band of AgNPs. This "blue" band was insensitive to the changes in the extent of the plasmonic coupling between the core AgNPs and the satellite AuNPs for separations down to ∼1 nm. When the core and the satellite nanoparticles are closer than ∼1 nm, the changes in the frequency of the coupling bands do not fit the classical electrodynamics model (GMM theory) predictions, suggesting that bridging or quantum effects are significant in this strong coupling regime. A new band abruptly appears between the "red" and "blue" band at a ∼1 nm gap that can be assigned as a charge-transfer plasmon. Controlled plasmon coupling was achieved through changes in the number of satellite AuNPs as well. Experimental and theoretical investigations showed that both "red" and "blue" bands red-shift with an increasing number of satellites. In particular, excitation of the LSPR of the core AgNP mediated by the LSPR of the surrounding AuNPs significantly contributes to the red-shift of the "red" band as the number of the satellites increases.

EXPERIMENTAL AND THEORETICAL METHODS

The Ag core−Au satellite nanoassemblies were prepared using the selective desorption approach previously reported.[22] The assembly process consists of five steps. The first step for the assembly (step 1) was to clean a glass slide (25 mm × 12 mm) and coat the surface of the glass with amine using (3-

dx.doi.org/10.1021/jz400602f | J. Phys. Chem. Lett. 2013, 4, 1371−1378

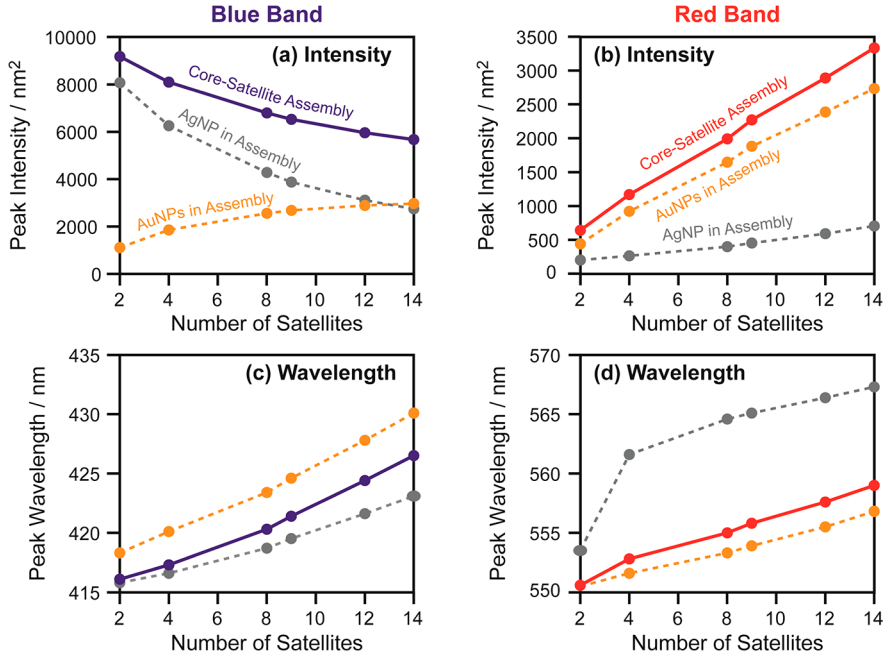

Figure 5. Changes in the peak intensities and frequencies of the calculated extinction spectra of Ag core−Au satellite nanoassemblies with increasing number of satellites. Blue and red circles indicate the changes of the "blue" band and the "red" band in the overall extinction spectra, respectively. Each spectrum was decomposed into the contributions of the component AgNP (gray circles) and AuNPs (yellow circles) in the assembly.

aminopropyl)trimethoxysilane (APTMS).[50] Then, the AgNPs (diameter 50 ± 4 nm), purchased from Ted Pella, were adsorbed onto the glass surface by immersing the glass slide in a AgNP solution (26 pM, 5 mL) for 12 h (step 2). To attach satellite AuNPs to the AgNPs on the glass, the AgNPs were functionalized with thiol using alkanedithiol (step 3). Immersion of the AgNP-adsorbed glass slides in alkanedithiol solutions (1 mM, 5 mL) for 12 h leads to the formation of highly ordered SAMs of alkanedithiol on the AgNP surfaces.[51] One exception was 1,2-ethanedithiol. Because of the formation of bilayers, the immersion time was limited to 1 h.[22,52] The core-to-satellite distances are readily adjusted by using various lengths of alkanedithiol, $SH(CH_2)_nSH$ (n = 2, 4, 6, 8, 10, 16), in this step. In the ensuing step (step 4), the AgNP-adsorbed glass slides were immersed in a AuNP solution (4 nM, 5 mL, AuNP = 13 ± 1 nm). Adsorption of the AuNPs on the thiol-functionalized AgNP surfaces led to the formation of core−satellite nanoassembly structures on the glass slides. The immersion time determines how many AuNPs adsorb on the AgNP surfaces. Note that the citrate-stabilized AuNPs adsorb on both the thiol-functionalized AgNPs and the amine-coated glass slides. However, ultrasonication of the slide in ethanol for 30 s exclusively desorbs the core−satellite nanoassemblies into the ethanol (step 5). For additional stability of the assembly, we exchanged the citrate on the satellites with mercaptoundecanoic acid (MUA) before step 5 by incubating the slides in MUA solution (1 mM, 5 mL) for 4 h. The structures and plasmonic couplings of the prepared core−satellite nanoassemblies were measured using a TEM (JEM-2100F, JEOL) and a UV−vis spectrometer (Lambda 25, PerkinElmer), respectively.

The optical response of Ag core−Au satellites was calculated using the GMM theory developed by Xu.[53−55] The GMM method provides a rigorous solution to the classical electromagnetic problem of light scattering by a cluster of non-overlapping spheres. In the GMM method, the total field upon each sphere is expanded in vector spherical harmonics and consists of two parts: the initial incident plane wave and the scattered waves from all of the other spheres in the cluster. Once the total field of the cluster is determined, one can readily calculate absorption, scattering, and extinction cross sections. Additionally, the various cross sections of the whole cluster can be decomposed into individual contributions from each sphere as previously described.[54,55]

To model the core−satellite structures in the experiment, the diameters of the AgNP and AuNP were set to 50 and 13 nm, respectively. The surface-to-surface distances between the core and satellites were estimated based on calculations of the length of the alkanedithiol linkers as in the previous work.[22] The number of AuNP satellites was chosen to be consistent with TEM observations, up to 14 satellites per core. (See Figure S3 in the Supporting Information.) The dielectric constants of Ag and Au were taken from Johnson and Christy[56] and modified to account for surface scattering of the electrons on the sphere boundaries.[57] The refractive index of the surrounding medium (ethanol) is fixed at 1.36. To mimic the stochastic positions of the Au satellites and their orientation with respect to the cores in the experiments, we generated batches of structures randomly in a way that maintained the core−satellite distance but allowed the relative positions of the satellites to vary. The results from each batch of simulations were then averaged to provide the final results.

■ ASSOCIATED CONTENT

Ⓢ Supporting Information

More discussion on the Fano resonance in Ag core−Au satellite nanoassemblies, TEM images of the assemblies with various alkanedithiol linkers, difficulties in measuring interparticle distances using TEM, and linear fitting of the red-shifts in the extinction spectrum of the assemblies with an increasing number of satellites. This material is available free of charge via the Internet at http://pubs.acs.org.

dx.doi.org/10.1021/jz400602f | J. Phys. Chem. Lett. 2013, 4, 1371−1378

AUTHOR INFORMATION

Corresponding Author

*E-mail: schatz@chem.northwestern.edu (G.C.S.), sangwoon@dankook.ac.kr (S.Y.).

Author Contributions

§Jun Hee Yoon and Yong Zhou contributed equally.

Notes

The authors declare no competing financial interest.

ACKNOWLEDGMENTS

This research was supported by the Basic Science Research Program through the National Research Foundation of Korea (NRF) funded by the Ministry of Education, Science and Technology (2010-0007764). Y.Z. and G.C.S. were supported by the Department of Energy, Basic Energy Sciences under grant DE-SC0004752. M.G.B. and G.C.S. were supported by the Northwestern Materials Research Center, NSF grant DMR-1121262. Computing resources were provided by the Quest high performance computing facility at Northwestern University.

REFERENCES

(1) Kelly, K. L.; Coronado, E.; Zhao, L. L.; Schatz, G. C. The Optical Properties of Metal Nanoparticles: The Influence of Size, Shape, and Dielectric Environment. *J. Phys. Chem. B* **2003**, *107*, 668−677.

(2) Jain, P. K.; Huang, X.; El-Sayed, I. H.; El-Sayed, M. A. Noble Metals on the Nanoscale: Optical and Photothermal Properties and Some Applications in Imaging, Sensing, Biology, and Medicine. *Acc. Chem. Res.* **2008**, *41*, 1578−1586.

(3) Giannini, V.; Fernández-Domínguez, A. I.; Heck, S. C.; Maier, S. A. Plasmonic Nanoantennas: Fundamentals and Their Use in Controlling the Radiative Properties of Nanoemitters. *Chem. Rev.* **2011**, *111*, 3888−3912.

(4) Mayer, K. M.; Hafner, J. H. Localized Surface Plasmon Resonance Sensors. *Chem. Rev.* **2011**, *111*, 3828−3857.

(5) Ross, M. B.; Blaber, M. G.; Schatz, G. C. Plasmonically Enhanced Dye-Sensitized Solar Cells. In *Plasmonics: Theory and Applications*; Shahbazyan, T. V., Stockman, M. I., Eds.; Springer Series Challenges and Advances in Computational Chemistry and Physics; Springer: Berlin, in press.

(6) Chen, H.; Schatz, G. C.; Ratner, M. A. Experimental and Theoretical Studies of Plasmon-Molecule Interactions. *Rep. Prog. Phys.* **2012**, *75*, 096402.

(7) Jones, M. R.; Osberg, K. D.; Macfarlane, R. J.; Langille, M. R.; Mirkin, C. A. Templated Techniques for the Synthesis and Assembly of Plasmonic Nanostructures. *Chem. Rev.* **2011**, *111*, 3736−3827.

(8) Halas, N. J.; Lal, S.; Chang, W.-S.; Link, S.; Nordlander, P. Plasmons in Strongly Coupled Metallic Nanostructures. *Chem. Rev.* **2011**, *111*, 3913−3961.

(9) Romo-Herrera, J. M.; Alvarez-Puebla, R. A.; Liz-Marzán, L. M. Controlled Assembly of Plasmonic Colloidal Nanoparticle Clusters. *Nanoscale* **2011**, *3*, 1304−1315.

(10) Rechberger, W.; Hohenau, A.; Leitner, A.; Krenn, J. R.; Lamprecht, B.; Aussenegg, F. R. Optical Properties of Two Interacting Gold Nanoparticles. *Opt. Commun.* **2003**, *220*, 137−141.

(11) Reinhard, B. M.; Siu, M.; Agarwal, H.; Alivisatos, A. P.; Liphardt, J. Calibration of Dynamic Molecular Rulers Based on Plasmon Coupling between Gold Nanoparticles. *Nano Lett.* **2005**, *5*, 2246−2252.

(12) Jain, P. K.; Huang, W.; El-Sayed, M. A. On the Universal Scaling Behavior of the Distance Decay of Plasmon Coupling in Metal Nanoparticle Pairs: A Plasmon Ruler Equation. *Nano Lett.* **2007**, *7*, 2080−2088.

(13) Prodan, E.; Radloff, C.; Halas, N. J.; Nordlander, P. A Hybridization Model for the Plasmon Response of Complex Nanostructures. *Science* **2003**, *302*, 419−422.

(14) Nordlander, P.; Oubre, C.; Prodan, E.; Li, K.; Stockman, M. I. Plasmon Hybridization in Nanoparticle Dimers. *Nano Lett.* **2004**, *4*, 899−903.

(15) Shanthil, M.; Thomas, R.; Swathi, R. S.; Thomas, K. G. Ag@SiO_2 Core-Shell Nanostructures: Distance-Dependent Plasmon Coupling and SERS Investigation. *J. Phys. Chem. Lett.* **2012**, *3*, 1459−1464.

(16) Sebba, D. S.; Lazarides, A. A. Robust Detection of Plasmon Coupling in Core-Satellite Nanoassemblies Linked by DNA. *J. Phys. Chem. C* **2008**, *112*, 18331−18339.

(17) Cheng, L.; Song, J.; Yin, J.; Duan, H. Self-Assembled Plasmonic Dimers of Amphiphilic Gold Nanocrystals. *J. Phys. Chem. Lett.* **2011**, *2*, 2258−2262.

(18) Bai, L.; Ma, X.; Liu, J.; Sun, X.; Zhao, D.; Evans, D. G. Rapid Separation and Purification of Nanoparticles in Organic Density Gradients. *J. Am. Chem. Soc.* **2010**, *132*, 2333−2337.

(19) Chen, G.; Wang, Y.; Tan, L. H.; Yang, M.; Tan, L. S.; Chen, Y.; Chen, H. High-Purity Separation of Gold Nanoparticle Dimers and Trimers. *J. Am. Chem. Soc.* **2009**, *131*, 4218−4219.

(20) Wang, Y.; Chen, G.; Yang, M.; Silber, G.; Xing, S.; Tan, L. H.; Wang, F.; Feng, Y.; Liu, X.; Li, S.; et al. A Systems Approach Towards the Stoichiometry-Controlled Hetero-Assembly of Nanoparticles. *Nat. Commun.* **2010**, *1*, 87.

(21) Zanchet, D.; Micheel, C. M.; Parak, W. J.; Gerion, D.; Williams, S. C.; Alivisatos, A. P. Electrophoretic and Structural Studies of DNA-Directed Au Nanoparticle Groupings. *J. Phys. Chem. B* **2002**, *106*, 11758−11763.

(22) Yoon, J. H.; Lim, J.; Yoon, S. Controlled Assembly and Plasmonic Properties of Asymmetric Core-Satellite Nanoassemblies. *ACS Nano* **2012**, *6*, 7199−7208.

(23) Kleinman, S. L.; Sharma, B.; Blaber, M. G.; Henry, A.-I.; Valley, N.; Freeman, R. G.; Natan, M. J.; Schatz, G. C.; Van Duyne, R. P. Structure Enhancement Factor Relationships in Single Gold Nanoantennas by Surface-Enhanced Raman Excitation Spectroscopy. *J. Am. Chem. Soc.* **2013**, *135*, 301−308.

(24) Pompa, P. P.; Martradonna, L.; Torre, A. D.; Sala, F. D.; Manna, L.; Vittorio, M. D.; Calabi, F.; Cingolani, R.; Rinaldi, R. Metal-Enhanced Fluorescence of Colloidal Nanocrystals with Nanoscale Control. *Nat. Nanotechnol.* **2006**, *1*, 126−130.

(25) Linic, S.; Christopher, P.; Ingram, D. B. Plasmonic-Metal Nanostructures for Efficient Conversion of Solar to Chemical Energy. *Nat. Mater.* **2011**, *10*, 911−921.

(26) Sheikholeslami, S.; Jun, Y.-W.; Jain, P. K.; Alivisatos, A. P. Coupling of Optical Resonances in a Compositionally Asymmetric Plasmonic Nanoparticle Dimer. *Nano Lett.* **2010**, *10*, 2655−2660.

(27) Prodan, E.; Nordlander, P. Plasmon Hybridization in Spherical Nanoparticles. *J. Chem. Phys.* **2004**, *120*, 5444−5454.

(28) Bachelier, G.; Russier-Antoine, I.; Benichou, E.; Jonin, C.; Fatti, N. D.; Vallée, F.; Brevet, P.-F. Fano Profiles Induced by Near-Field Coupling in Heterogeneous Dimers of Gold and Silver Nanoparticles. *Phys. Rev. Lett.* **2008**, *101*, 197401.

(29) Encina, E. R.; Coronado, E. A. On the Far Field Optical Properties of Ag-Au Nanosphere Pairs. *J. Phys. Chem. C* **2010**, *114*, 16278−16284.

(30) Encina, E. R.; Coronado, E. A. Near Field Enhancement in Ag Au Nanospheres Heterodimers. *J. Phys. Chem. C* **2011**, *115*, 15908−15914.

(31) Peña-Rodríguez, O.; Pal, U.; Campoy-Quiles, M.; Rodríguez-Fernández, L.; Garriga, M.; Alonso, M. I. Enhanced Fano Resonance in Asymmetrical Au:Ag Heterodimers. *J. Phys. Chem. C* **2011**, *115*, 6410−6414.

(32) Gunnarsson, L.; Rindzevicius, T.; Prikulis, J.; Kasemo, B.; Käll, M.; Zou, S.; Schatz, G. C. Confined Plasmons in Nanofabricated Single Silver Particle Pairs: Experimental Observations of Strong Interparticle Interactions. *J. Phys. Chem. B* **2005**, *109*, 1079−1087.

(33) McMahon, J. M.; Gray, S. K.; Schatz, G. C. Optical Properties of Nanowire Dimers with a Spatially Nonlocal Dielectric Function. *Nano Lett.* **2010**, *10*, 3473−3481.

(34) Esteban, R.; Borisov, A. G.; Nordlander, P.; Aizpurua, J. Bridging Quantum and Classical Plasmonics with a Quantum-Corrected Model. *Nat. Commun.* **2012**, *3*, 825.
(35) Sönnichsen, C.; Reinhard, B. M.; Liphardt, J.; Alivisatos, A. P. A Molecular Ruler Based on Plasmon Coupling of Single Gold and Silver Nanoparticles. *Nat. Biotechnol.* **2005**, *23*, 741−745.
(36) Hill, R. T.; Mock, J. J.; Hucknall, A.; Wolter, S. D.; Jokerst, N. M.; Smith, D. R.; Chilkoti, A. Plasmon Ruler with Angstrom Length Resolution. *ACS Nano* **2012**, *6*, 9237−9246.
(37) Su, K.-H.; Wei, Q.-H.; Zhang, X.; Mock, J. J.; Smith, D. R.; Schultz, S. Interparticle Coupling Effects on Plasmon Resonances of Nanogold Particles. *Nano Lett.* **2003**, *3*, 1087−1090.
(38) Sebba, D. S.; Mock, J. J.; Smith, D. R.; LaBean, T. H.; Lazarides, A. A. Reconfigurable Core-Satellite Nanoassemblies as Molecularly-Driven Plasmonic Switches. *Nano Lett.* **2008**, *8*, 1803−1808.
(39) Peng, S.; McMahon, J. M.; Schatz, G. C.; Gray, S. K.; Sun, Y. Reversing the Size-Dependence of Surface Plasmon Resonances. *Proc. Natl. Acad. Sci. U.S.A.* **2010**, *107*, 14530−14534.
(40) McMahon, J. M.; Gray, S. K.; Schatz, G. C. Nonlocal Optical Response of Metal Nanostructures with Arbitrary Shape. *Phys. Rev. Lett.* **2009**, *103*, 097403.
(41) McMahon, J. M.; Gray, S. K.; Schatz, G. C. Calculating Nonlocal Optical Properties of Structures with Arbitrary Shape. *Phys. Rev. B* **2010**, *82*, 035423.
(42) Toscano, G.; Raza, S.; Jauho, A.-P.; Mortensen, N. A.; Wubs, M. Modified Field Enhancement and Extinction by Plasmonic Nanowire Dimers Due to Nonlocal Response. *Opt. Express* **2012**, *20*, 4176−4188.
(43) Zhao, L. L.; Jensen, L.; Schatz, G. C. Surface-Enhanced Raman Scattering of Pyrazine at the Junction between Two Ag_{20} Nanoclusters. *Nano Lett.* **2006**, *6*, 1229−1234.
(44) Aikens, C. M.; Schatz, G. C. TDDFT Studies of Absorption and SERS Spectra of Pyridine Interacting with Au_{20}. *J. Phys. Chem. A* **2006**, *110*, 13317−13324.
(45) Slaughter, L.; Chang, W.-S.; Link, S. Characterizing Plasmons in Nanoparticles and Their Assemblies with Single Particle Spectroscopy. *J. Phys. Chem. Lett.* **2011**, *2*, 2015−2023.
(46) Slaughter, L. S.; Wu, Y.; Willingham, B. A.; Nordlander, P.; Link, S. Effects of Symmetry Breaking and Conductive Contact on the Plasmon Coupling in Gold Nanorod Dimers. *ACS Nano* **2010**, *4*, 4657−4666.
(47) Ross, B. M.; Waldeisen, J. R.; Wang, T.; Lee, L. P. Strategies for Nanoplasmonic Core-Satellite Biomolecular Sensors: Theory-Based Design. *Appl. Phys. Lett.* **2009**, *95*, 193112.
(48) Yoon, J. H.; Yoon, S. Effects of the Number of Satellites on Surface Plasmon Coupling of Core-Satellite Nanoassemblies. *Bull. Korean Chem. Soc.* **2013**, *34*, 33−34.
(49) Rouhana, L. L.; Moussallem, M. D.; Schlenoff, J. B. Adsorption of Short-Chain Thiols and Disulfides onto Gold under Defined Mass Transport Conditions: Coverage, Kinetics, and Mechanism. *J. Am. Chem. Soc.* **2011**, *133*, 16080−16091.
(50) Freeman, R. G.; Grabar, K. C.; Allison, K. J.; Bright, R. M.; Davis, J. A.; Guthrie, A. P.; Hommer, M. B.; Jackson, M. A.; Smith, P. C.; Walter, D. G.; et al. Self-Assembled Metal Colloid Monolayers: An Approach to SERS Substrates. *Science* **1995**, *267*, 1629−1632.
(51) Rieley, H.; Kendall, G. K.; Zemicael, F. W.; Smith, T. L.; Yang, S. X-Ray Studies of Self-Assembled Monolayers on Coinage Metals. 1. Alignment and Photooxidation in 1,8-Octanedithiol and 1-Octanethiol on Au. *Langmuir* **1998**, *14*, 5147−5153.
(52) Joo, S. W.; Han, S. W.; Kim, K. Multilayer Formation of 1,2-Ethanedithiol on Gold: Surface-Enhanced Raman Scattering and Ellipsometry Study. *Langmuir* **2000**, *16*, 5391−5396.
(53) Xu, Y.-l. Electromagnetic Scattering by an Aggregate of Spheres. *Appl. Opt.* **1995**, *34*, 4573−4588.
(54) Xu, Y.-l. Electromagnetic Scattering by an Aggregate of Spheres: Far Field. *Appl. Opt.* **1997**, *36*, 9496−9508.
(55) Xu, Y.-l.; Wang, R. T. Electromagnetic Scattering by an Aggregate of Spheres: Theoretical and Experimental Study of the Amplitude Scattering Matrix. *Phys. Rev. E* **1998**, *58*, 3931−3948.
(56) Johnson, P. B.; Christy, R. W. Optical Constants of the Noble Metals. *Phys. Rev. B* **1972**, *6*, 4370−4379.
(57) Kreibig, U.; Fragstein, C. V. The Limitation of Electron Mean Free Path in Small Silver Particles. *Z. Phys.* **1969**, *224*, 307−323.